Diamond & Related Materials 18 (2009) 979–983

Contents lists available at ScienceDirect

Diamond & Related Materials

journal homepage: www.elsevier.com/locate/diamond

Designing of carbon nanofilaments-based composites for innovative applications

Federico Cesano, Serena Bertarione, Domenica Scarano *, Giuseppe Spoto, Adriano Zecchina

Department of IFM Chemistry, University of Torino, NIS Centre of Excellence, Center of Reference INSTM, Via Pietro Giuria 7, 10125 Torino, Italy

ARTICLE INFO

Available online 27 November 2008

Keywords:
Polymer composites
Nanofibres
Nanostructures
CVD

ABSTRACT

The catalytic growth of CNTs and/or CNFs polymer composites has been performed by means of the chemical vapour deposition of a C_2H_4/H_2 gas mixture on polymer supports (i.e. para-aramide powders and fibres) at 500–600 °C. By selecting suitable reaction parameters, the concentration and the growth level of the CNTs and/or CNFs on the polymer surface can be changed, according to the final properties of the obtained composite. Nanofilaments, 20÷120 nm in diameter formed at 500 °C on polymer supported Ni catalysts, give rise, at first, to a carbon-polymer composite. A more dense porous nanotissue, then generated at 600 °C, embeds the polymer substrate with formation of a carbon-carbon composite. In this work, the progressive formation of carbon-polymer and then carbon-carbon composites is investigated by SEM, TEM and AFM microscopies and by XRD analysis.

1. Introduction

Carbon based composites have attracted a great attention in recent years due to the wide applicability to many fields, including catalytic supports, gas storage, porous membranes and electrodes [1–5]. Among these, carbon nanotubes (CNTs) and/or carbon nanofibres (CNFs) have been found extremely attractive in view of their use as reinforcing "fillers" for materials or for forming structural or functional innovative composite materials [6,7]. In particular CNTs/CNFs on the surface of organic polymers have been found particularly promising to improve properties such as oxidation resistance and/or electrical conductivity [8,9]. Moreover the presence of CNTs/CNFs on a polymer powder facilitates subsequent processing steps, like extrusion of the granules into fibres or films. According to known methods, CNTs/CNFs are synthesized on intermediate substrates and then mixed with polymers [10]. To overcome the disadvantages of this complex method, which requires the removal of the intermediate substrate, the aim of the present work is to show a simple way for the '*in-situ*' catalytic growth of CNTs/CNFs [11] on para-aramide substrates, which are known to have high elastic modulus, low specific density, high thermal and chemical resistances. The catalytic method requires metal nanoparticles (usually Ni, Fe, or Co or alloys) [2,12] supported on the substrates and a carbon feedstock (hydrocarbon, CO). Metal catalysts are well known to be active in forming C-nanostructures and to reduce the pyrolysis temperature, with a large carbon yield [13,14]. It is commonly accepted that the reaction proceeds at the exposed surface of the metal and that the diameter of the carbon filaments produced catalytically is related to the diameter of the metal particles [12,15]. As the formation of the porous network is governed by the synthesis conditions, in this work the formation and the catalytic growth of a carbon matrix on polymer powders and fibres supports is followed by means of SEM, TEM, AFM microscopies and XRD analysis.

2. Experimental

The polymer substrates used in this work, constituted by para-aramide powder (Twaron 5011) or fibres (Twaron 3360 dTex type 1000), have been impregnated with solutions 0.5M of $Ni(NO_3)_2 \cdot 6H_2O$ salt in ethanol by an incipient wetness impregnation process followed by evaporation (120 °C) and calcination in air (300 °C). These substrates, located in a cylindrical quartz furnace, were contacted with: i) 100 ml/min N_2 flow gas up to 400 °C at atmospheric pressure; ii) a pure H_2 flow gas (100 ml/min) for 15 min at 400 °C. After raising the temperatures in H_2 up to 500 °C, 550 °C (*results not reported for sake of brevity*) and 600 °C, the samples were then contacted with a H_2/C_2H_4 gas mixture (4:1 volumetric ratio) for 60 min. By adopting this procedure, carbon yields up to 200% and 400%, have been quantified on powder and fibres supports for samples obtained at 600 °C, respectively.

Thermal analyses (TGA with a 100 ml/min N_2 flow gas and TPD with a 100 ml/min He flow gas, both up to 800 °C at atmospheric pressure) of the para-aramide polymer powders and fibres have been carried out, in order to investigate their thermal stability.

Polymer supports and composites have been characterized by scanning electron microscopy (SEM, Leica Cambridge Stereoscan 420 instrument, equipped with an energy dispersive X-ray spectroscopy (EDX), by TEM (Jeol 2000EX instrument 200KeV), by AFM (Park Scientific Instrument Auto Probe LS). The crystallinity of the samples has been estimated by XRD analysis (X-ray diffractometer with Ni filtered CuKα radiation using a standard Bragg–Brentano geometry).

* Corresponding author. Department of IFM Chemistry, University of Torino, Via Pietro Giuria 7, 10125 Torino, Italy. Tel.: +39 0116707834; fax: +39 0116707855.
E-mail address: domenica.scarano@unito.it (D. Scarano).

0925-9635/$ – see front matter © 2008 Elsevier B.V. All rights reserved.
doi:10.1016/j.diamond.2008.11.011

3. Results and discussion

TGA and DTGA (Fig. 1a) analyses on the samples evidence narrow and intense features at 560 °C and 571 °C for the powder and fibres samples respectively, due to the thermal decomposition of the materials. On the fibre sample a broad and low intense DTGA peak is observed too in the 45 °C–130 °C range, due to the dehydration process. This peak is negligible on powder samples.

From TPD analyses (Fig. 1b) two distinct temperature ranges are observed: (i) the first one (at 80–150 °C), well evidenced on the fibre sample (bottom in Fig. 1b), is dominated by water and CO losses; (ii) the second one (at 450–800 °C), observed on both powders (Fig. 1a) and fibres (Fig. 1b), is characterized by the simultaneous evolution of several volatile species (H_2O, CO, CO_2, C_6H_6, C_7H_8, C_7H_5N..), which reveals that the dominant process is the polymer degradation. Notice that this feature is occurring at higher temperatures on fibres supports. From the comparison of TGA and TPD data, it results that the fibre support is slightly more stable than the powder one toward the thermal decomposition.

Fig. 2a–f reports SEM, TEM and XRD images related to the powder sample before and after the the growth of nanofilaments at 500 °C and 600 °C. The SEM micrographs of the starting sample (Fig. 2a and inset therein) show a complex tangle of particles aggregates, not easily distinguishable. From XRD pattern (Fig. 2d) two main diffraction peaks at $2\theta\cong20{,}5°$ and at $2\theta\cong22{,}9°$ corresponding to the (110) and (200) planes of the orthorhombic crystalline structure of the polymeric material are evidenced, together with minor peaks at $2\theta\cong27{,}9°$ and at $2\theta\cong42{,}9°$ ascribed to (210) and (220) planes of the Twaron polymer [16]. Due to the quite high value of the full width at half maximum (FWHM) of the main features, it comes out that the crystalline degree of the powder support is modest (*vide infra*). SEM images in Fig. 2b (and inset bottom right) illustrate the presence of a network of nanofilaments interconnecting and covering uniformly the polymer particles, which appear irregularly shaped, with dimensions ranging from a few microns to 20 μm. From TEM image (inset top right in Fig. 2b) beside nickel particles, nanofibres about 20 nm in diameter and 300–400 nm in length, which escaped the SEM observation, are observed at the surface of "free" metal particles with diameter in the same interval. The corresponding XRD pattern (Fig. 2e) reveals, beside the two diffraction peaks with maxima at $2\theta\cong25{,}9°$ (narrow and intense) and at $2\theta\cong43{,}4°$ (broad and weak), respectively assigned to the (002) planes and to the (100)/(101) planes convolution of turbostratic carbon phases [17], minor features (shoulders on the left side of the (002) carbon peak) due to the (110) and (200) planes of the polymer particles. These features confirm the formation of a carbon-polymer composite made of a porous network of carbon nanofilaments embedding the polymer particles. Furthermore other peaks at $2\theta\cong44{,}5°$ and at $2\theta\cong51{,}9°$, ascribed to (111) and (200) planes of cubic Ni particles, are evidenced. From the peak broadening and by using the Scherrer's equation $d = K\lambda/(\beta\cos\theta)$ (where d is the mean grain size, λ is the X-ray wavelenght, β is the FWHM of the diffraction line, corrected by the instrumental broadening, θ means the diffraction angle and K is a constant, which has been assumed to be 0.9 for the cubic case and 1.54 for the hexagonal one), the size of scattering coherent domains have been calculated [18]. From this, it comes out that the main grain size of the cubic Nickel crystals, (obtained from the (111) direction), is about 12 nm.

On the sample treated at 600 °C (Fig. 2c and inset therein) particles aggregates, embedded in a more dense porous network of nanofilaments, about 100÷200 nm in diameter and a few microns long, are formed. It is noteworthy that the size of these nanofilaments is depending on the temperature of synthesis. As a matter of fact by comparing Fig. 2b and c (SEM/TEM images of the samples obtained at 500 °C and 600 °C on polymer powder used as support) a remarkable increase in the diameter of the nanofilaments is observed: from about 20 nm (500 °C) to 100÷200 nm (600 °C).

From XRD pattern (Fig. 2f) the features due to (002) planes and to the (100)/(101) planes convolution of turbostratic carbon phases are

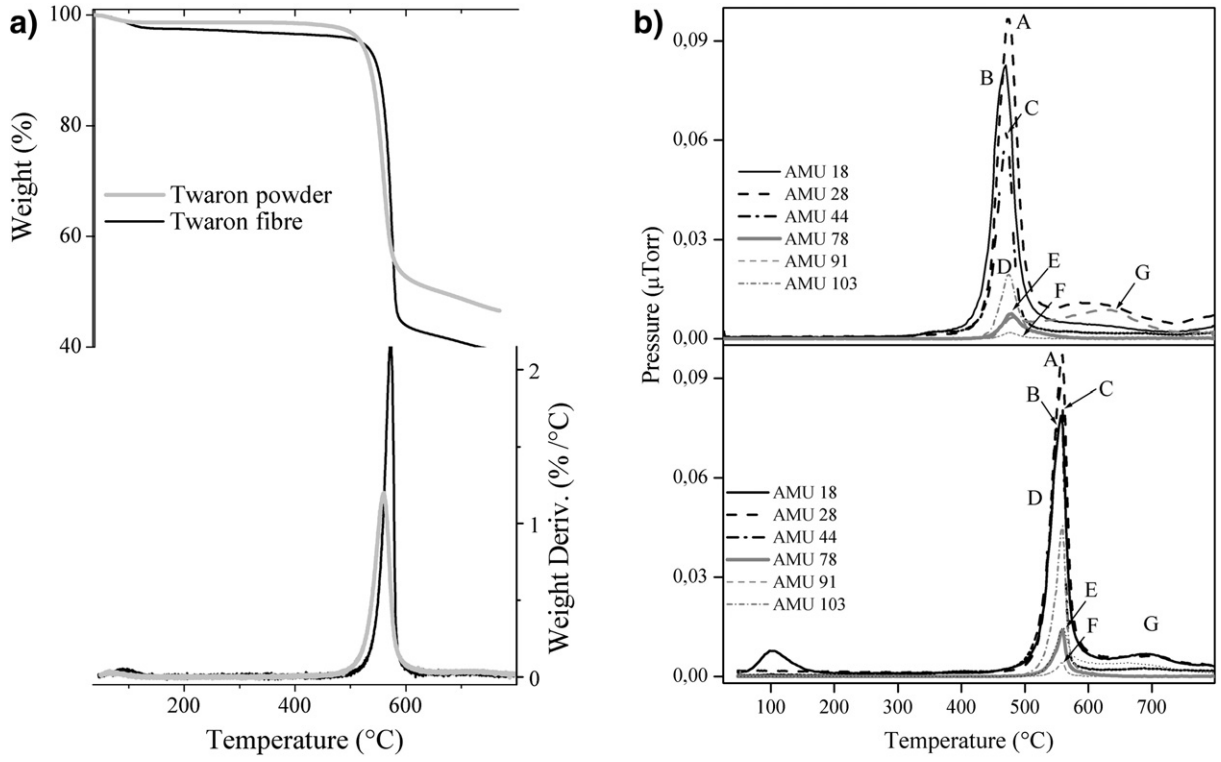

Fig. 1. Thermal analyses of polymer support. a) TGA (on the top) and DTGA (on the bottom): powder (light grey lines), fibre (black lines); b) TPD of powders (on the top) and fibres (on the bottom). According to the atomic mass units (AMUs), the evolving species have been reported: N_2/CO (A), H_2O (B), CO_2 (C), C_6H_5CN (D), benzene (E), toluene (F) and HCN(G).

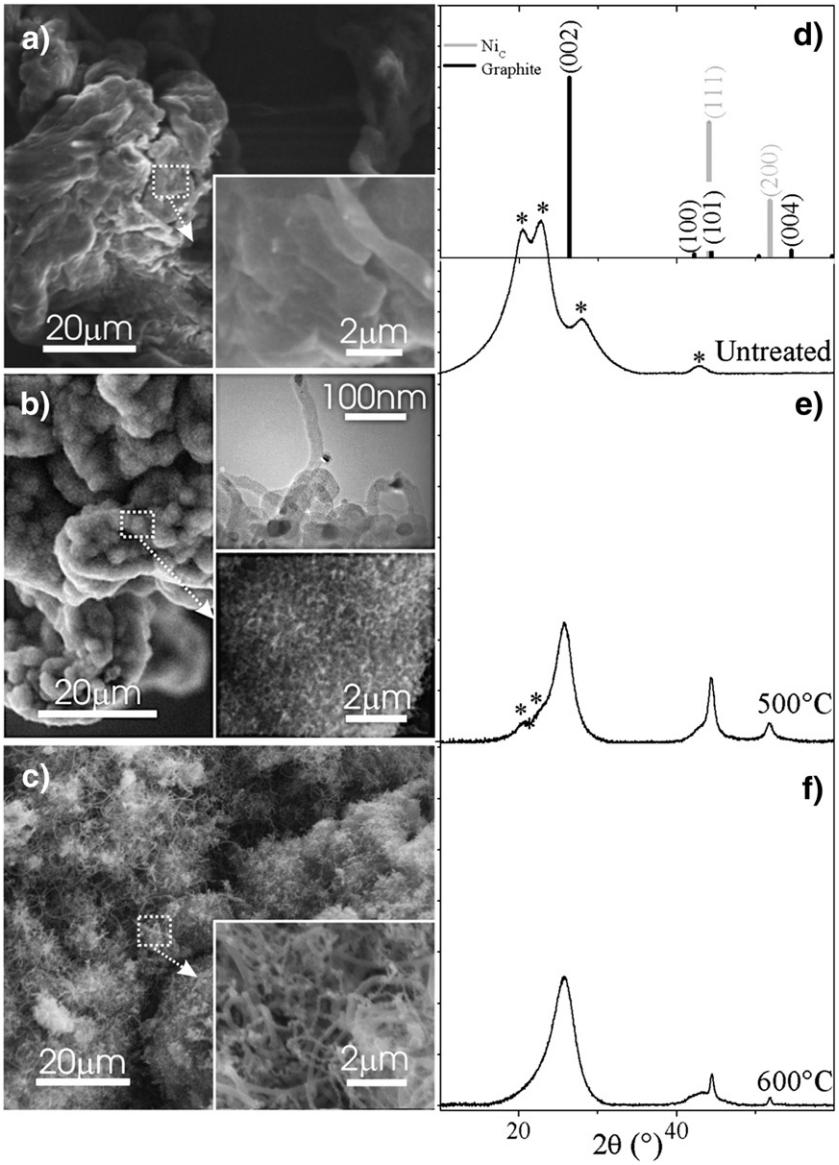

Fig. 2. a) b) c) SEM images of polymer powder used as support and samples obtained at 500 °C and 600 °C, respectively. In the insets (bottom on the right), enlarged views of the selected areas in a), b) and c), are shown; b) (inset on the top right): one carbon nanofilament is HRTEM imaged. d) e) f) XRD patterns of polymer powder, and samples obtained at 500 °C and 600 °C, respectively. The diffraction lines of reference materials are reported: Twaron polymers (*) and cubic Ni phases (light grey).

becoming predominant, whereas the absence of planes due to polymer support is confirming the polymer degradation in this temperature range, as expected from thermal analyses (Fig. 1).

Coming now to analogous experiments made on the fibre support, SEM image in Fig. 3a, as well as the enlarged view (inset in the right bottom part of Fig. 3a), show that the sample is constituted by a collection of nearly parallel and regular commercial fibres (Twaron 3360 dTex type 1000), characterized by regular dimensions (~10–12 μm in diameter) and by uniform and flat surface. In Fig. 3a, the smooth character of the fibres surface is further evidenced by AFM (inset in the right upper part of the image).

From XRD analysis (Fig. 3d), well defined diffraction peaks corresponding to the (110), (200) crystalline planes of the polymer are observed, which reveals that the fibres show a higher degree of crystallinity with respect to the powder system.

In Fig. 3b and c SEM micrographs of portions of the sample after the syntheses at 500 °C and 600 °C, respectively, are shown. From Fig. 3b (and inset therein) a higher roughness of the fibres surface can be evidenced as compared to that one of the starting material. Beside nickel particles agglomerates (*vide infra*), uniformly dispersed on the fibres surface, a few nanofilaments emerging from the polymer fibre could be observed. In particular from the profile of a fibre located in a more external position (i.e. without a second one in vicinal place) one protruding nanofilament, about 120 nm in diameter and less than 2 μm long, is imaged.

As before discussed, for samples obtained at 500 °C, the same is occurring moving from Fig. 3a to b. In this case the diameter is increasing from about 50 nm (500 °C) to 150÷300 nm (600 °C) as well. AFM image (inset in Fig. 3b for sample at 600 °C) is confirming this result.

Due to the low amount of CNTs/CNFs synthesized under these conditions, no diffraction peaks corresponding to the graphitic carbon can be detected from the XRD pattern (Fig. 3e). Otherwise, the relevant presence of peaks, associated with the (110), (200) and (210) typical crystalline planes of the Twaron fiber is highlighted, thus testifying the crystalline character of the fibre support. Notice that

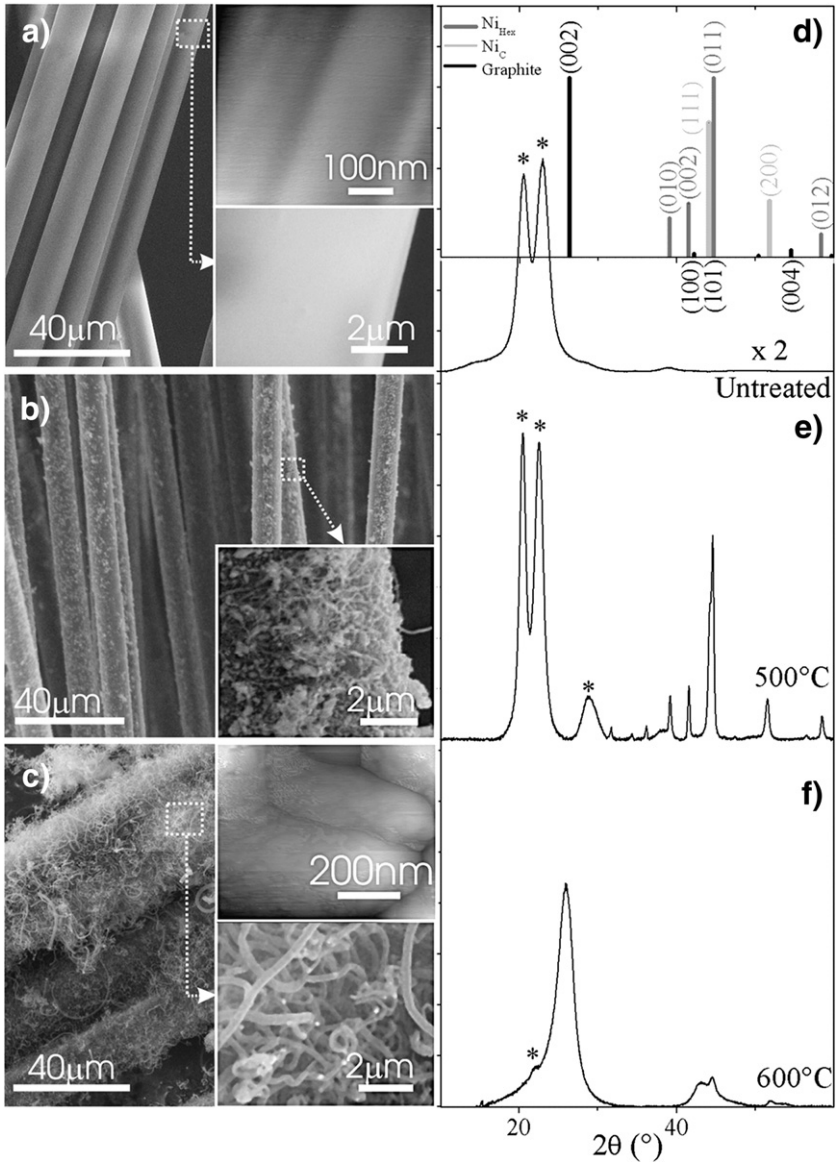

Fig. 3. a) b) c) SEM and AFM images of polymer fibres used as support and samples obtained at 500 °C and 600 °C, respectively. In the insets (bottom on the right) enlarged views of the selected areas in a), b) and c), are SEM imaged. In the insets (top on the right) enlarged views of the selected areas in a) and c) are AFM imaged. d) e) f) XRD patterns of polymer fibres and samples obtained at 500 °C and 600 °C, respectively. The diffraction lines of reference materials are reported: Twaron polymers (*), hexagonal Ni phases (grey) and cubic Ni phases (light grey).

moving from the starting polymer (Fig. 3d) to the annealed sample (Fig. 3e), the relative intensity and width of the (110) and (200) polymer main peaks are changing, which implies a modification of the sample crystallinity [19]. This can be further confirmed by thermal analyses (Fig. 1a,b), where mass losses due to the formation of volatile products were expected to cause changes in crystallinity.

On the XRD pattern of the sample treated at 500 °C (Fig. 3e), further features at $2\theta \cong 39{,}2°$, $2\theta \cong 41{,}6°$, $2\theta \cong 44{,}6°$, $2\theta \cong 58{,}6°$ associated with the (010), (002), (011) and (012) planes of the nickel hexagonal phase and at $2\theta \cong 44{,}5°$ and at $2\theta \cong 51{,}9°$ associated with the (111) and (200) planes of the nickel cubic phase are observed. These features are confirming the crystalline nature of the metal agglomerates, as imaged from SEM. By using the before discussed Scherrer's formula, the grain sizes of the nickel crystallites are calculated to be 72 nm (from the cubic (111) direction) and 116 nm (from the hexagonal (010) direction), respectively. These values are remarkably different as compared to those on powders; this can be explained with a different dispersion degree of the nickel particles on powder and fibre supports.

From SEM image of the sample at 600 °C (Fig. 3c) a complex network of nanofilaments, more than 2 μm long, with 150÷300 nm approximate diameters, is interconnecting two originally independent fibres. Evidence of the formation of nanofilaments comes also from AFM image (inset in the right upper part of Fig. 3c), where a portion of two curved nanofilaments is highlighted.

From this picture (and in the inset as well), it is possible to appreciate more clearly the presence, along and at the end of the filaments, of metal particles with approximately 100÷200 nm diameter, which play a critical role in favoring the progressive formation of the porous stage [7].

It is noteworthy that by moving from the powder to fibres used as support, the size of the nanofilaments can be observed to increase in a remarkable way, this being explained with the different values of the specific surface area of the different supports. A powder system with a higher surface area with respect to a fibre support is favouring, at first, a better dispersion of the catalyst particles (Ni or Fe), then the nucleation and growth of many structures homogeneously distributed. The

formation of a porous nanotissue is confirmed by XRD data (Fig. 3f), because, beside minor features ascribed to (111) and (200) planes of cubic nickel crystals, the two main diffraction peaks assigned to the (002) and (100) planes of carbon phases, are evidenced. In particular, the (002) peak, as compared to the same observed on powder polymer, shows a smaller value of the FWHM, typical of a more high graphitization degree of the C-matrix. It is noteworthy that the high level of graphitization of the obtained composite is comparable to that of a carbon fibre commercially available and obtained through pyrolysis at high temperature [7].

4. Conclusions

The catalytic method affords an effective way to synthesize under mild conditions (500 °C) carbon nanofilaments on polymer based supports giving rise to carbon-polymer composites, which then can be transformed to carbon-carbon materials, in a low temperature range (500 °C–600 °C). The role of the support in promoting the formation of the nanofilament network is highlighted. This means that the surface area of the original supports (powder, fibres) may play a vital role for the dispersion of the catalyst precursor on the support, so affecting the growth of the nanofilaments.

In particular powder supports favour the formation, at 500 °C of a porous network of nanofilaments, characterized by a low graphitization degree and low weight percentage yield. Otherwise fibre supports promote the formation, at 600 °C of a porous nanotissue, constituted by intercrossing nanofilaments characterized by a high graphitization degree and high weight percentage yield.

Acknowledgements

The authors thank MIUR, INSTM Consorzio and NANOMAT Project for their economical support.

References

[1] J.D. Buckley, Ed. Handbook of Composites, Chapman & Hall, London, 1998.
[2] K.P. De Jong, J.W. Geus, Catal. Rev.-Sci. Eng. 42 (2000) 481.
[3] F. Cesano, D. Scarano, S. Bertarione, F. Bonino, A. Damin, S. Bordiga, C. Prestipino, C. Lamberti, A. Zecchina, J. Photochem. Photobiol. A-Chem. 196 (2008) 143.
[4] F. Cesano, E. Groppo, F. Bonino, A. Damin, C. Lamberti, S. Bordiga, A. Zecchina, Adv. Mater. 18 (2006) 3111.
[5] F. Cesano, S. Bertarione, A. Damin, G. Agostini, S. Usseglio, V. Jenny, C. Lamberti, G. Spoto, D. Scarano, A. Zecchina, Adv. Mater. 20 (2008) 3342.
[6] V.P. Veedu, A.Y. Cao, X.S. Li, K.G. Ma, C. Soldano, S. Kar, P.M. Ajayan, M.N. Ghasemi-Nejhad, Nat. Mater. 5 (2006) 457.
[7] F. Cesano, S. Bertarione, D. Scarano, A. Zecchina, Chem. Mat. 17 (2005) 5119.
[8] S. Hofmann, C. Ducati, B. Kleinsorge, J. Robertson, Appl. Phys. Lett. 83 (2003) 4661.
[9] E.S. Choi, J.S. Brooks, D.L. Eaton, M.S. Al-Haik, M.Y. Hussaini, H. Garmestani, D. Li, K. Dahmen, J. Appl. Phys. 94 (2003) 6034.
[10] G.X. Chen, Y.J. Li, H. Shimizu, Carbon 45 (2007) 2334.
[11] M. Cantoro, V.B. Golovko, S. Hofmann, D.R. Williams, C. Ducati, J. Geng, B.O. Boskovic, B. Kleinsorge, D.A. Jefferson, A.C. Ferrari, B.F.G. Johnson, J. Robertson, Diam. Relat. Mat. 14 (2005) 733.
[12] K.B.K. Teo, C. Singh, Chhowalla, W.I. Milne, in: H.S. Nalwa (Ed.), Encyclopedia of Nanoscience and Nanotechnology, Vol. I, American Scientific Publishers, Cambridge, 2004, p. 665.
[13] H. Okuno, M. Trinquecoste, A. Derre, M. Monthioux, P. Delhaes, J. Mater. Res. 17 (2002) 1904.
[14] N.I. Maksimova, O.P. Krivoruchko, G. Mestl, V.I. Zaikovskii, A.L. Chuvilin, A.N. Salanov, E.B. Burgina, J. Mol. Catal. A-Chem. 158 (2000) 301.
[15] S. Helveg, C. Lopez-Cartes, J. Sehested, P.L. Hansen, B.S. Clausen, J.R. Rostrup-Nielsen, F. Abild-Pedersen, J.K. Norskov, Nature 427 (2004) 426.
[16] A. Castro-Muniz, A. Martinez-Alonso, J.M.D. Tascon, Carbon 46 (2008) 985.
[17] A. Cuesta, P. Dhamelincourt, J. Laureyns, A. Martynez-Alonso, J.M.D. Tascon, J. Mat. Chem. 8 (1998) 2875.
[18] L.S. Birks, H. Friedman, 17 (1946) 687.
[19] A.M. Hindeleh, A.A.A. Obaid, Acta Polym. 47 (1996) 55.